Inorganic Chemistry

pubs.acs.org/IC

Article

Magnetically Driven Quantum Phase Transition in a Low-Dimensional Pyrazine-Bridged Cu^{2+} Chain Magnet

Avery L. Blockmon,◆ Jinhyeong Jo,◆ Kiman Park, Emma Kirkman-Davis, Mark M. Turnbull, Minseong Lee, John Singleton, Stephen A. McGill, Heung-Sik Kim, Jun Hee Lee,* and Janice L. Musfeldt*

Cite This: *Inorg. Chem.* 2025, 64, 12518−12526

Read Online

ACCESS | Metrics & More | Article Recommendations | Supporting Information

ABSTRACT: The magnetic properties and phase diagrams of $S = 1/2$ quasi-one-dimensional Heisenberg antiferromagnets are well-established with copper-containing coordination polymers as the platform of choice due to their low energy scales and ease of chemical substitution. The inability to uncover orbitally resolved components of the magnetization has, however, been a long-standing barrier to greater understanding of high field spin state transitions. In this work, we combine pulsed field magnetization, optical spectroscopy, and magnetic circular dichroism with complementary electronic structure calculations to unravel orbital-specific contributions to the magnetism in the linear chain quantum magnet $[CuL_2(H_2O)_2(pyz)](ClO_4)_2$ [L = 5-methyl-2-pyridone; pyz = pyrazine]. In addition to revealing a spin flop and field-driven transition to the fully saturated spin state, we untangle the green → teal color change across the 185 K structural phase transition and employ what we learn about the different Cu^{2+} → pyrazine charge transfer excitations to decompose the magnetic circular dichroism. Analysis reveals that both e_g-derived Cu^{2+} 3*d* orbitals play a role in the field-driven transition to the fully saturated state, not just those formally hosting unpaired electrons. We attribute the surprisingly strong dichroic signature at room temperature to the presence of uncorrelated spin.

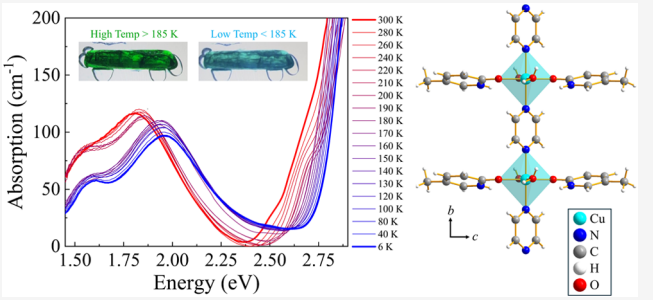

INTRODUCTION

Molecule-based materials are well-known for their complex energy landscapes, sensitivity to external stimuli, and property control via chemical substitution. Copper-containing coordination polymers in particular host an extraordinary number of competing phases and properties.[1−4] These systems offer an edge to researchers interested in the fundamental aspects of quantum magnetism. Their smaller exchange interactions, for instance, allow magnetization to be saturated in experimentally available fields.[5−13] This is just one example of how small external perturbations can change important energy scales, driving into new states with very different properties.[14,15] Molecule-based quantum magnets also provide a framework for exploring magnetic topology, chiral spin textures, and atomic clock transitions[16−18] as well as developing antiferromagnets and altermagnets for fast, low power, nonvolatile RAM and state-of-the-art spintronics devices.[19−23]

Our work focuses on a pyrazine-bridged Cu^{2+} chain that belongs to the class of $S = 1/2$ quasi-one-dimensional Heisenberg antiferromagnets. This family of materials hosts intriguing magnetic behavior, magnetostructural correlations, and magnetic field−temperature ($H-T$) phase diagrams of foundational interest.[24] $Cu(pyz)(NO_3)_2$ is a notable example. This linear chain magnet has well-isolated spin chains that give rise to long-range ordering, spin canting, and a saturation field of 14 T.[9,25−27] Other Cu^{2+} spin chains include Cs_2CuCl_4 where magnetic frustration induces complex magnetic ordering,[28,29] $(CH_3)_2CHNH_3CuCl_3$ that undergoes a thermochromic transition from brown to orange,[30] chiral $[Cu(pym)(H_2O)_4]$-$SiF_6{\cdot}H_2O$ with high field polarization, magnetoelectric coupling, and exotic magnetic field−temperature phase diagrams,[31] and the $Cu(pyz)(pyO)_2(H_2O)_x(PF_6)_2$ family of materials (x = 0, 2) where changing the ratio of starting materials modifies product dimensionality.[32] Clearly, pyrazine-bridged Cu^{2+} chains are widely employed to uncover a variety of different properties.

Our work concentrates on $[CuL_2(H_2O)_2\ (pyz)](ClO_4)_2$ [L = 5-methyl-2-pyridone; pyz = pyrazine] [Figure 1(a)].[33] Susceptibility reveals antiferromagnetic interactions with $J = -9.2$ K between Cu centers, and magnetization displays a slight upward curvature, although higher fields are needed to

Received: January 31, 2025
Revised: April 29, 2025
Accepted: May 19, 2025
Published: June 12, 2025

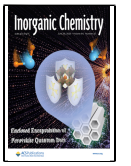

https://doi.org/10.1021/acs.inorgchem.5c00458
Inorg. Chem. 2025, 64, 12518−12526

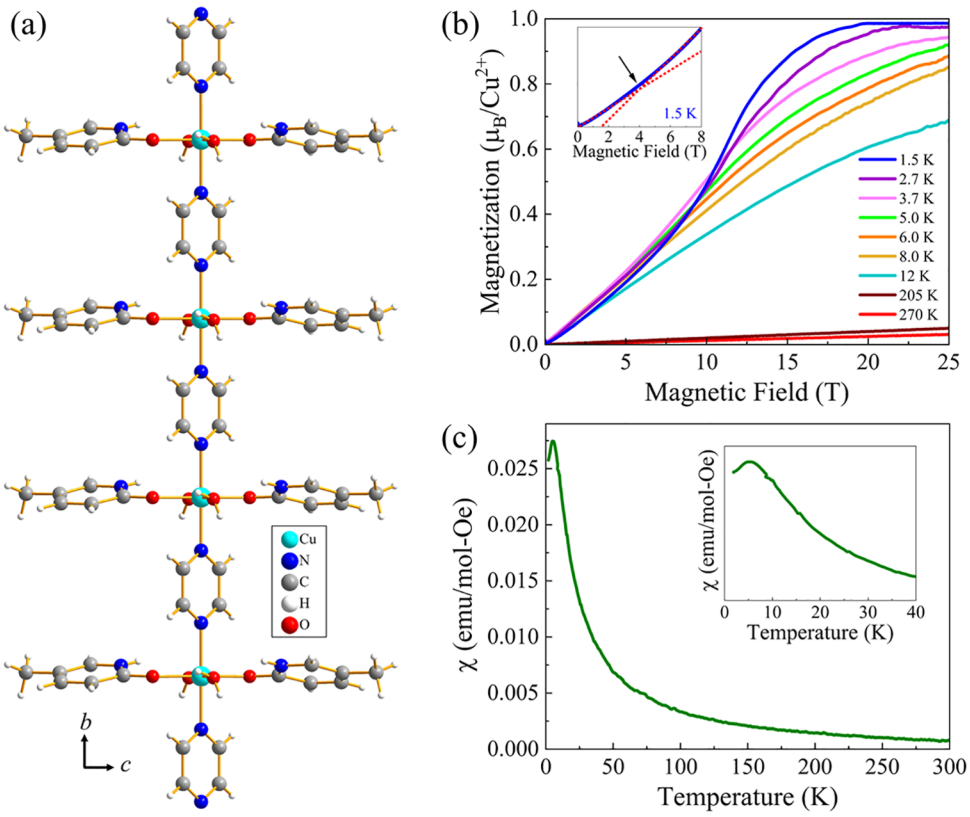

Figure 1. (a) Ball and stick representation of $[CuL_2(H_2O)_2(pyz)](ClO_4)_2$ where L is 5-methyl-2-pyridone and pyz is pyrazine. Perchlorate counterions are omitted for clarity. (b) Pulsed field magnetization at several different temperatures in the $H\perp b$ configuration. Inset: Close-up view of the magnetization at 1.5 K revealing a possible spin-flop transition near 4 T. (c) Magnetic susceptibility as a function of temperature. Inset: Close-up view of the susceptibility.

determine the saturation field.[33] This system also hosts a structural phase transition near 185 K that is accompanied by a beautiful green to teal color change.[33] As might be anticipated from the color properties, the transition metal center resides in a distorted octahedral environment with a Jahn−Teller elongation along the Cu−OH_2 axis.[33] The space group in the high temperature phase is $C2/c$ whereas that in the low temperature phase is $P\bar{1}$.[33] Remarkably, the Cu^{2+} environment is more distorted at high (rather than low) temperatures[33,34]—a situation that presents interesting opportunities for unraveling the orbital character of a quantum magnet.

In this work, we combine optical spectroscopy and magnetic circular dichroism with magnetization and first-principles calculations to uncover the properties of the linear chain antiferromagnet $[CuL_2(H_2O)_2(pyz)](ClO_4)_2$. Analysis reveals that the color change and structural phase transition are due to a sharp shift in the Cu^{2+} → pyrazine charge transfer excitation. In addition to being a perfect illustration of local structure and crystal field effects, thermochromic materials are used in sensors, smart windows, quality assurance packaging, and other technologies requiring visual temperature indicators.[35−37] We also find a 4 T spin flop and transition to the fully saturated spin state near 20 T. Magnetic circular dichroism across these field-induced transitions uncovers orbitally resolved components of the magnetization. It turns out that both of the Cu^{2+} e_g-derived orbitals participate in the transition to the fully saturated spin state. We discuss these results in terms of the charge transfer excitations in this class of quantum magnets and the similarity between traditional and "optical" magnetization. This likeness implies that the excited state hosts limited field dependence.

RESULTS AND DISCUSSION

Magnetic Properties of $[CuL_2(H_2O)_2(pyz)](ClO_4)_2$. Figure 1(b,c) summarizes the magnetization and magnetic susceptibility of $[CuL_2(H_2O)_2(pyz)](ClO_4)_2$ in the $H\perp b$ configuration. There is long-range antiferromagnetic ordering near 1.2 K, a maximum in the susceptibility at 5.5 K,[33] a possible spin flop near 4 T, and a field-driven transition to the fully saturated spin state at approximately 20 T. This behavior is typical of an $S = 1/2$ quantum antiferromagnet,[5] and it places the magnetic energy scales of this system on a solid footing from which we can better understand the magnetic circular dichroism spectroscopy. Similar data for the $H\|b$ configuration are given in Figure S1, Supporting Information.

Color Properties across the Structural Phase Transition. Figure 2(a) displays the optical absorption of $[CuL_2(H_2O)_2(pyz)](ClO_4)_2$ as a function of temperature. The most striking aspect is the way the color bands shift to higher energies across the 185 K structural phase transition. Materials that absorb light at 1.85 eV have a perceived complementary color of green, whereas those that absorb near 1.95 eV are seen as cyan or teal.[38] This implies that the abrupt shift in the absorption (and the excitations and orbitals that the spectra represent) is responsible for the green → teal color change across the structural phase transition. Our first-principles calculations simulate the differences between the high ($C2/c$) and low ($P\bar{1}$) temperature phase spectra very well

https://doi.org/10.1021/acs.inorgchem.5c00458
Inorg. Chem. 2025, 64, 12518−12526

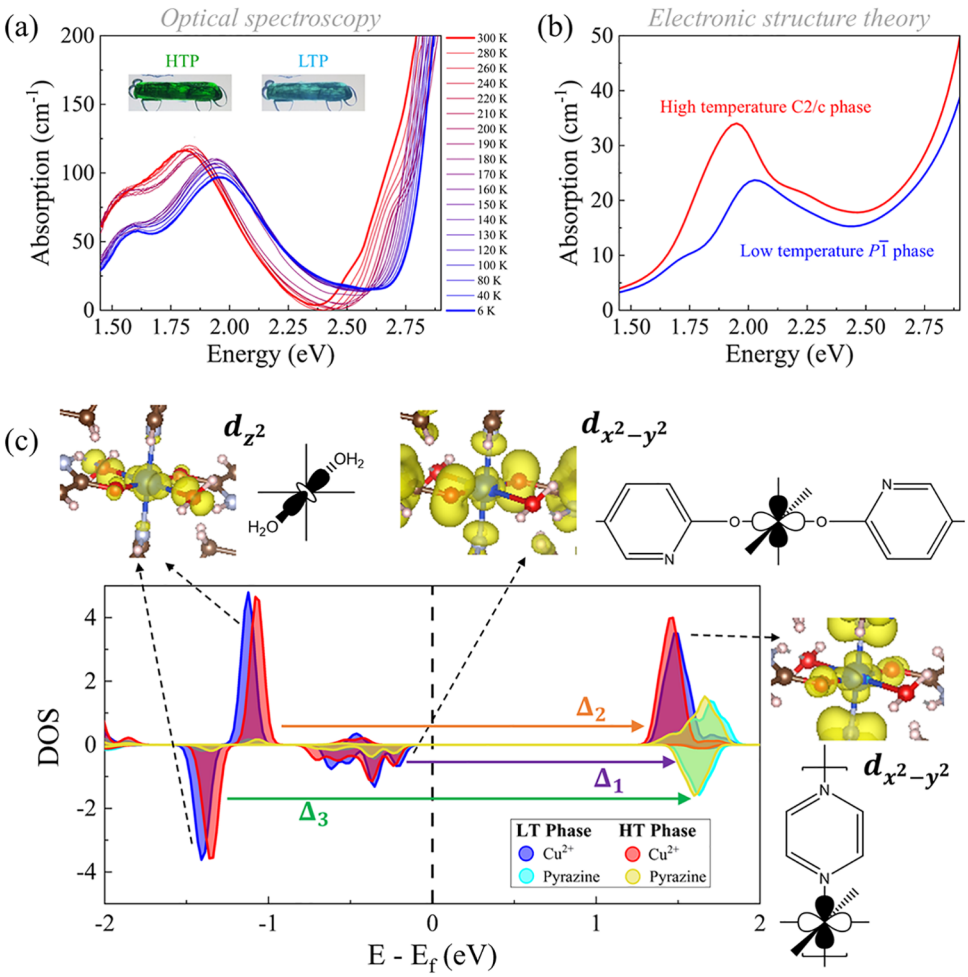

Figure 2. (a, b) Measured and simulated optical absorption spectra of $[CuL_2(H_2O)_2(pyz)](ClO_4)_2$ where L is 5-methyl-2-pyridone as a function of temperature. Photographs of the crystals are included for comparison. (c) Spin-projected density of states (DOS) for both the high and low temperature phases. The direction of the Jahn−Teller elongation places the energies of the d_{z^2} and $d_{x^2-y^2}$ orbitals closest to the Fermi level. Each of the colored arrows represents a different type of excitation as discussed in the text.

[Figure 2(b)] placing the system on a firm foundation for additional analysis.

Figure 2(c) summarizes the spin-projected density of states in the high and low temperature phases of $[CuL_2(H_2O)_2(pyz)](ClO_4)_2$. This rendering reveals the specific Cu^{2+} orbitals that contribute to the optical properties and, at the same time, allows us to more deeply understand the symmetry conditions and crystal field environment. Analysis of the partial charge density confirms that the Cu^{2+} orbitals contributing to the excitations between 1.4 and 3.0 eV are e_g-derived structures: d_{z^2} and $d_{x^2-y^2}$.[39] The $d_{x^2-y^2}$ orbital has significant overlap with the pyrazine and oxy-5-methyl-2-pyridone ligands. In particular, the $d_{x^2-y^2}$ and pyrazine orbitals form the lowest unoccupied band and thus represent the "final state" for all electronic excitations in this energy range. This band therefore plays a major role in determining the optical properties of $[CuL_2(H_2O)_2(pyz)](ClO_4)_2$. Since it hosts the unpaired spin, $d_{x^2-y^2}$ is the "magnetic orbital" as well. With these symmetry considerations in mind, we can analyze and assign the most important spectral features in Figure 2(a). There are three primary excitations:

1. $d_{x^2-y^2}$ → pyrazine charge transfer in the spin-down channel (Δ_1, purple arrow),
2. d_{z^2} → pyrazine charge transfer in the spin-up channel combined with the d_{z^2} to $d_{x^2-y^2}$ on-site excitation (Δ_2, orange arrow), and
3. d_{z^2} → pyrazine charge transfer in the spin-down channel (Δ_3, green arrow).

Only the first pathway Δ_1 is predicted to take place at energies below 2 eV. Changes in the Cu^{2+} $d_{x^2-y^2}$ → pyrazine charge transfer excitation in the spin-down channel are thus responsible for the green → teal color variation across the structural phase transition.

Magnetic Circular Dichroism Yields an Orbitally Decomposed Optical Magnetization. Figure 3 summarizes the magnetic circular dichroism of $[CuL_2(H_2O)_2(pyz)](ClO_4)_2$. Focusing first on the low temperature $P\bar{1}$ phase [Figure 3(a)], we see that the full field spectrum hosts two modestly sized features near 1.4 and 1.7 eV, a broad asymmetric structure with a maximum near 2.1 eV, and an even larger feature near 2.8 eV. Based upon our first-principles calculations, we assign the features below 2 eV as Cu^{2+} $d_{x^2-y^2}$ → pyrazine charge transfer in the spin-down channel, the broad structure centered at 2.1 eV as emanating from d_{z^2} → pyrazine charge transfer in the spin-up channel combined with d_{z^2} to $d_{x^2-y^2}$ on-site excitations, and the peak near 2.8 eV as due to d_{z^2} → pyrazine charge transfer in the spin-down channel. There

https://doi.org/10.1021/acs.inorgchem.5c00458
Inorg. Chem. 2025, 64, 12518−12526

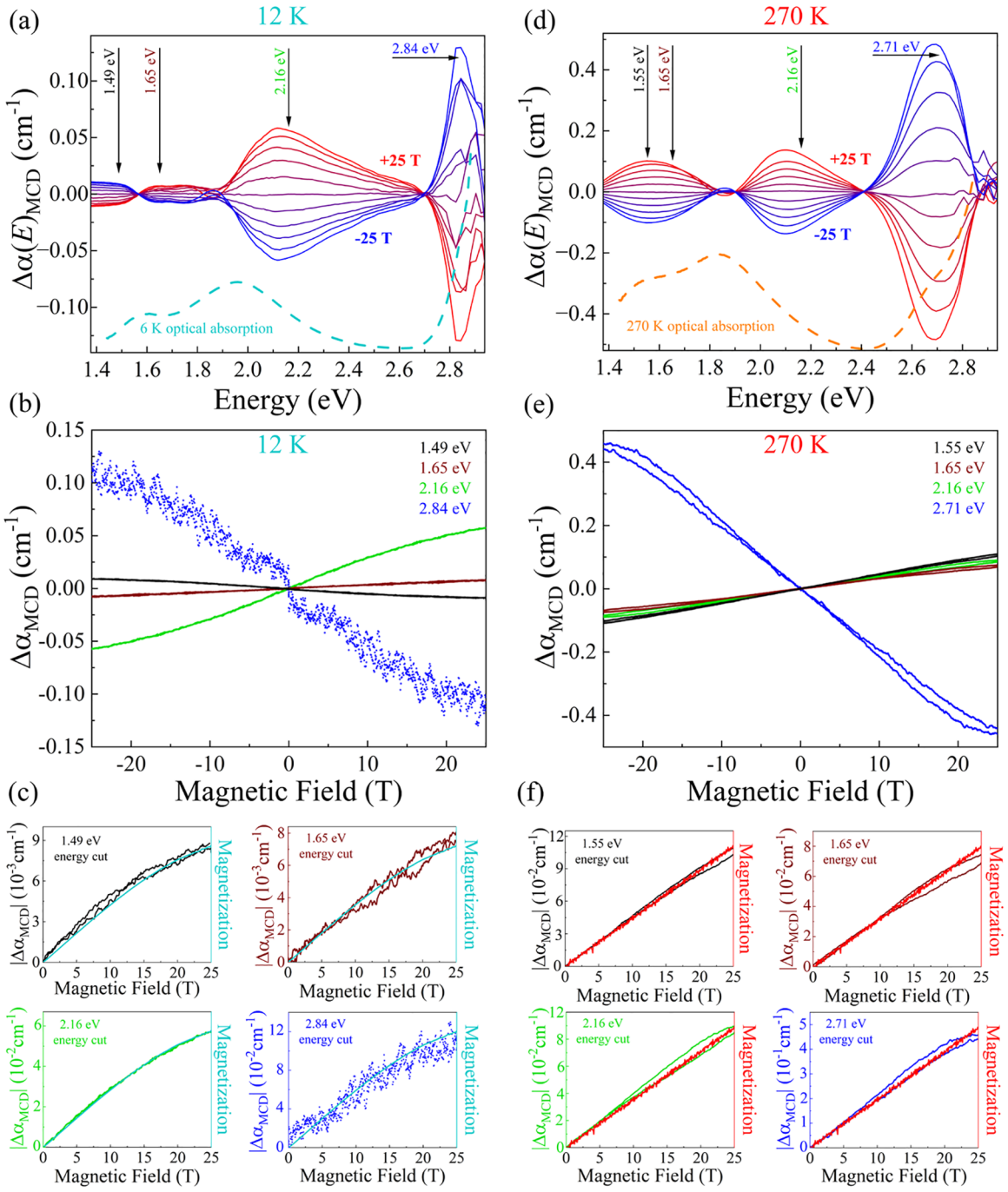

Figure 3. (a) Magnetic circular dichroism of $[CuL_2(H_2O)_2(pyz)](ClO_4)_2$ from +25 to −25 T at 12 K. The absolute absorption is shown below for reference. (b) Overlay of the optical magnetization at specific energies, obtained from the data in (a). (c) Double *y*-axis plots of the absolute value of the optical and traditional magnetization at 12 K. (d) Magnetic circular dichroism from +25 to −25 T at 270 K. The absolute absorption spectrum is shown for comparison. (e) Overlay of different optical magnetization curves at specific energy cuts taken at 270 K. (f) Double *y*-axis plots comparing the optical and traditional magnetization at 270 K. The optical magnetization is given by $\Delta\alpha_{MCD}$. Constant energy cuts of this quantity (as indicated by arrows in panels (a, d)) allow us to explore the role of individual orbitals.

are three isosbestic points, where the values of the up- and down-spin density of states are identical. Similar structures appear in the high temperature ($C2/c$ phase) dichroic response [Figure 3(d)]. The assignments are the same, although the band positions are slightly different.

Importantly, features in the dichroic spectra, $\Delta\alpha(E)_{MCD}$, are directly proportional to net magnetization, and since we can analyze this effect at different energies, the response can be correlated with specific metal centers, certain aspects of the joint density of states, or even to specific bands and orbitals.[40−43] These relationships are expressed as:

$$\Delta\alpha(E)_{MCD} = \vec{\mu}_i \cdot \vec{k} = |\vec{\mu}_i||\vec{k}|\cos\theta \approx \frac{(\alpha_+(E) - \alpha_-(E))d}{2} \approx \frac{\Delta E}{2}\frac{1}{\alpha(E)}\frac{d\alpha(E)}{dE} \quad (1)$$

https://doi.org/10.1021/acs.inorgchem.5c00458
Inorg. Chem. 2025, 64, 12518−12526

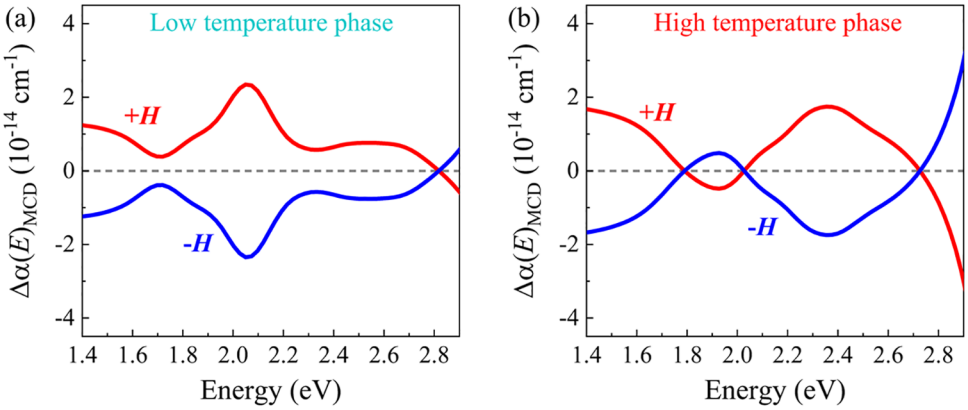

Figure 4. Simulated dichroic spectra of $[CuL_2(H_2O)_2(pyz)](ClO_4)_2$ where L is 5-methyl-2-pyridone in (a) the low temperature ($P\bar{1}$) phase and (b) high temperature ($C2/c$) phase from first-principles calculations. Both positive ($+H$) and negative ($-H$) fields are shown.

Here, $\Delta\alpha(E)_{MCD}$ is the absorption difference between right and left circularly polarized light ($\alpha_+(E) - \alpha_-(E)$), $d\alpha(E)/dE$ is the energy derivative of the linear absorption spectrum, d is the sample thickness, ΔE is the peak-to-peak energy difference, $\vec{\mu}_i$ is the magnetic moment projected onto the light propagation direction $\vec{k}$, and θ is the angle between the magnetic moment and the light propagation. The moment is proportional to magnetic field. Equation 1 nicely highlights the first-derivative relationship between the linear absorption and magnetic circular dichroism. Any inflection point in the linear absorption spectra will be amplified in the dichroic response [Figure 3(a,d)]. Magnetic circular dichroism is, of course, a well-known and sensitive probe of molecular symmetry. What is different here is that it is employed to unravel a spin state transition triggered by very high magnetic fields.

The arrows in Figure 3(a) mark the energies where we performed field sweeps of the dichroic response. These "optical magnetization" curves can be considered as a type of orbitally projected magnetism. Figure 3(b) reveals the behavior of the three types of excitations in the low temperature phase. The optical magnetization curve at 2.84 eV has the largest value—in line with the prominence of the feature in the dichroic spectrum that we assign as Cu^{2+} d_{z^2} → pyrazine charge transfer excitation in the spin-down channel. This curve also has the highest sensitivity to the remnant of the spin flop transition at 4 T. By contrast, the excitation at 2.16 eV is the most responsive to the magnetic saturation transition near 20 T, although because these experiments were performed at 12 K rather than below T_N, the transition is rounded rather than sharp.

We can also compare the results of our pulsed field magnetization [Figure 1(b)] with the optical magnetization curves [Figure 3(b)]. Given our assignments, the latter can be considered an orbitally projected magnetism, although it reflects the joint density of states between the ground and excited states. The comparison in Figure 3(c) is striking. We immediately notice that the optical magnetization is very similar to that in the ground state. This suggests that the majority of field dependence resides in the ground (rather then excited) state. We assign the optical magnetization curves based upon their energies according to the density of states plot in Figure 2(d). Again, the optical magnetization curves taken at 1.49 and 1.65 eV probe the behavior of Cu^{2+} $d_{x^2-y^2}$ to pyrazine charge transfer in the spin-down channel, that at 2.16 eV detects a combination of Cu^{2+} d_{z^2} to pyrazine charge transfer in the spin-up channel and d_{z^2} to $d_{x^2-y^2}$ on-site excitations, and the curve at 2.84 eV reflects the behavior of the Cu^{2+} d_{z^2} to pyrazine charge transfer in the spin-down channel. Based upon the agreement between the magnetization and constant energy cuts of the magnetic circular dichroism spectra, we find that all three excitations contribute to spin behavior in this system.

Figure 3(d) displays the magnetic circular dichroism spectra of $[CuL_2(H_2O)_2(pyz)](ClO_4)_2$ in the high temperature $C2/c$ phase at 270 K. Above 2 eV, the general shape is similar to that in the low-temperature phase except the largest structure is shifted to lower energy. This trend is consistent with what we see in the optical absorption spectra [Figure 2(a)]. The feature in the dichroic response near 2.1 eV is more symmetric than before, although it retains its uneven shape. The isosbestic point near 1.86 eV is also preserved. At lower energies, the dichroic spectra in Figure 3(d) are very different. For instance, there is a single relatively symmetric feature centered near 1.5 eV, whereas there are two smaller bands separated by another isosbestic point in the low temperature phase spectra. We attribute this effect to a slight shift of the spin-down density of states to lower energies at temperatures above the structural phase transition. The arrows in Figure 3(d) indicate the energies where we collected field sweep data. The latter gives the optical magnetization curves shown in Figure 3(e).

Figure 3(f) brings together the pulsed field magnetization and the absolute value of the optical magnetization. The overall agreement is excellent, implying that the excited state is not very field-dependent in the high temperature $C2/c$ phase either. The size of the optical magnetization is also substantial—even though there is no long-range ordering. The curve at 2.71 eV, which probes the contribution of the Cu^{2+} d_{z^2} to pyrazine charge transfer in the spin-down channel to the total magnetization, once again has the largest value, demonstrating that it is probably the most important. Even so, all of the optical magnetization curves follow the same trend revealing that both e_g-derived orbitals contribute to the net magnetism. Another unique aspect of the high temperature phase is that the optical magnetization at 2.71 eV displays a clear hysteresis. This behavior suggests that the excitation is capturing some type of sluggish field-induced process that is maximized around 20 T. Our calculations reveal that field-driven modifications to the spin state are accompanied by significant volume changes particularly in the high temperature phase. These effects may play a role in the process in the sense

https://doi.org/10.1021/acs.inorgchem.5c00458
Inorg. Chem. 2025, 64, 12518−12526

that hysteresis may be a consequence of high temperature phase volume (and perhaps atomic position) effects that take place on a slower time scale.

Turning back to Figure 1(b), the high temperature magnetization is very small which is to be expected when thermal energy dominates, yet we still see a large magneto-optical signal at 270 K [Figure 3(f)]. This is because magnetic circular dichroism is a local probe of electronic interactions involving the Cu^{2+} center whereas magnetization measures the bulk ground state response in a material. We therefore see that even upon approach to room temperature, the individual spins and electronic orbitals in this Cu-containing coordination polymer are robust and surprisingly sensitive to applied field even though they contribute little to the overall magnetization. This magnification of the magnetic circular dichroism may be enabled by structural changes across the 185 K transition that act to reduce entropy in combination with remnants of the field-induced spin-state crossover near 20 T.

Modeling the Dichroic Response of $[CuL_2(H_2O)_2(pyz)](ClO_4)_2$. We performed additional computational analysis to better understand and replicate the magnetic circular dichroism spectra of $[CuL_2(H_2O)_2(pyz)](ClO_4)_2$. As shown in Figure 4, the general shape aligns well, although the simulated results are shifted to higher energies compared to the experimental spectra. The calculated high temperature phase spectra have all of the same isosbestic points as the experimental data. This signifies that our model captures changes between the spin channels very well. On the other hand, the simulated dichroic spectrum in the low temperature phase displays only a bottleneck shape in the low energy region rather than a full isosbestic point or crossover. The general agreement is, however, more than sufficient to effectively interpret the dichroic response of quantum magnets like $[CuL_2(H_2O)_2(pyz)](ClO_4)_2$ and to analyze unusual entropy trends in the system.

SUMMARY

The magnetic properties and phase diagrams of $S = 1/2$ quasi-one-dimensional Heisenberg antiferromagnets are well-established and have attracted attention for decades. Copper-containing coordination polymers are the platform of choice for much of this work—primarily due to their low energy scales, ease of chemical substitution, and experimentally accessible critical fields. One barrier to greater understanding of these quantum magnets is the inability to uncover orbitally resolved components of the magnetization across a spin state transition. In this work, we take steps in this direction by combining optical spectroscopy and magnetic circular dichroism with magnetization and first-principles calculations to uncover the properties of the linear chain antiferromagnet $[CuL_2(H_2O)_2(pyz)](ClO_4)_2$. Analysis reveals that the green → teal color change across the 185 K $C2/c$ to $P\bar{1}$ structural phase transition is due to a sharp shift in the Cu^{2+} to pyrazine charge transfer excitation—a perfect illustration of local structure and crystal field effects. We also identify a possible spin flop at 4 T and a transition to the fully saturated spin state near 20 T and employ magnetic circular dichroism to unravel the orbitally resolved components of the magnetization. This procedure makes use of the overall low energy scales of this copper-containing coordination polymer, although the technique is broadly applicable to other magnetic materials. We find that orbital-specific magnetism involves both of the Cu^{2+} e_g-derived orbitals and is substantial even near room temperature although spin−spin correlations are obviously diminished.

METHODS

Crystal Growth and Sample Preparation. Single crystals of $[CuL_2(H_2O)_2(pyz)](ClO_4)_2$ where L = 5-methyl-2-pyridone were grown as described previously.[33] Crystals develop with a rod-like shape with the long direction corresponding to the crystallographic b-axis. To control the optical density, single crystals were hand-polished down to approximately 400 μm using fine-grit sand paper. To prevent the removal of waters of crystallization under vacuum and provide mechanical support for the high field work, we coated the crystals with clear ÅngströmBond 9110LV epoxy. The latter is completely transparent from approximately 1.1 to 3.4 eV making it well-suited for this work.

Magnetic Properties. Magnetic susceptibility was measured using a commercially available superconducting quantum interference device (SQUID) from Quantum Design. This setup utilizes a vibrating sample magnetometer, and measurements were taken in a dc field at 0.1 T between 1.9−300 K. Magnetization measurements were performed using a 65 T short-pulse magnet at the National High Magnetic Field Laboratory in Los Alamos, NM as described previously.[44] Data were collected between 1.2 and 270 K in the $H\|b$ and $H\perp b$ configurations. We calibrated the pulsed-field magnetization using data from the aforementioned SQUID measurements.

Optical Spectroscopy. A PerkinElmer λ-1050 grating spectrometer was used to measure transmittance in the bc plane from 1.4 to 3 eV. Transmittance is converted to absorption as $\alpha(E) = -\frac{1}{d}\ln(T(E))$. Here, $T(E)$ is the measured transmittance as a function of energy (E), and d is the sample thickness. An open-flow helium cryostat was employed for temperature control (4.2−300 K).

Dichroic Spectroscopy. Magnetic circular dichroism measurements were performed at the National High Magnetic Field Laboratory in Tallahassee, FL using the 25 T split helix magnet that has four wide window ports in the center of the magnet allowing for optical experiments.[45] Access to this magnet was crucial to this work, providing both direct optical access and a field high enough to saturate the magnetic state of interest. Measurements were taken with magnetic fields between +25 and −25 T using a 240 W Xe lamp measuring over an energy range between 1.37 and 3.10 eV in the Faraday geometry. Magnetic circular dichroism measures the difference between right- and left circularly polarized (RCP and LCP) light at different magnetic fields. The transmittance is then converted into absorption differences ($\Delta\alpha$) as detailed previously.[43] To enhance the signal-to-noise ratio, a chopper was utilized at a constant frequency, followed by a linear polarizer set at a 45° angle. Subsequently, a photoelastic modulator positioned after the linear polarizer cyclically converted the linearly polarized light into left or right circularly polarized light at regular intervals governed by $\delta(t) = \lambda/4\sin(\omega t)$. An optical fiber collected and directed the light to the detector while lock-in amplifiers were employed to separate all signals. MCD spectra were acquired at different temperatures, ranging from 12 to 270 K. Note that 12 K is the lower limit for the temperature range as the window ports affixed to the magnet that enable optical measurements allow some external energy inside the magnet as well. The high-temperature limit of 270 K was achieved by adding an additional heater to the sample probe.

First-Principles Calculations. The Vienna Ab Initio Simulation Package (VASP),[46,47] which implements the density functional theory + U (DFT + U) calculation method using the plane augmented wave method, was used for the optical analysis of $[CuL_2(H_2O)_2(pyz)](ClO_4)_2$. The initial structure of each phase was constructed based on the experimentally determined crystal structure.[33] We chose the local density approximation (LDA)[48] exchange-correlation functional form as the exchange functional. We used a $4 \times 4 \times 2$ k-point mesh for the low-temperature phase ($P\bar{1}$) and $4 \times 4 \times 1$ k-point mesh for the high-temperature phase $C2/c$ with kinetic energy cutoff of 500 eV to calculate the structure optimization and optical property. We set $U =$

https://doi.org/10.1021/acs.inorgchem.5c00458
Inorg. Chem. 2025, 64, 12518−12526

3.8 eV in the 3d orbital of Cu^{2+}. This U value shows the best results consistent with the experimental absorption results. We also tried setting different values of 4 and 3.5 eV to check the difference depending on the U value. We confirmed that there is a global shift depending on the value of U but that the transfer channel does not change. This revealed that changes in U value do not significantly affect the calculation results. To simulate the experimental results in which the magnetic field was applied, we performed all calculations assuming spins are aligned in the direction of the magnetic field. We implement the optical conductivity tensor to obtain the simulated magnetic circular dichroism spectra using the following equation[42,49]

$$\Delta\alpha_{MCD} \approx \frac{dw}{2c}\mathrm{Im}[n_+ - n_-] \approx \frac{2\pi d}{c}\mathrm{Im}\left[\frac{-\sigma_{xy}}{\left(1 + 1\frac{4\pi}{w}\sigma_{xx}\right)^{1/2}}\right] \quad (2)$$

Here, c is the speed of light, d is the thickness of the sample, and $n_\pm = (\epsilon_{xx} \pm \epsilon_{xy})^{1/2}$ is the refractive index for the right- and left-circularly polarized light. The dielectric functions were calculated using the exact diagonalization implanted in VASP.

■ ASSOCIATED CONTENT

Supporting Information

The Supporting Information is available free of charge at https://pubs.acs.org/doi/10.1021/acs.inorgchem.5c00458.

Magnetization measurements in the $H\|b$ direction, additional magnetic circular dichroism results, detailed discussion on the crystal field environment of $[CuL_2(H_2O)_2(pyz)](ClO_4)_2$, and more information about the DFT + U calculations (PDF)

■ AUTHOR INFORMATION

Corresponding Authors

Jun Hee Lee − *Department of Energy Engineering, Ulsan National Institute of Science and Technology, Ulsan 44919, Republic of Korea; Graduate School of Semiconductor Materials and Devices Engineering, Ulsan National Institute of Science and Technology, Ulsan 44919, Republic of Korea;* orcid.org/0000-0001-5121-244X; Email: junhee@unist.ac.kr

Janice L. Musfeldt − *Department of Chemistry, University of Tennessee, Knoxville, Tennessee 37996, United States; Department of Physics, University of Tennessee, Knoxville, Tennessee 37996, United States;* orcid.org/0000-0002-6241-823X; Email: Musfeldt@utk.edu

Authors

Avery L. Blockmon − *Department of Chemistry, University of Tennessee, Knoxville, Tennessee 37996, United States;* orcid.org/0000-0002-0951-9832

Jinhyeong Jo − *Department of Energy Engineering, Ulsan National Institute of Science and Technology, Ulsan 44919, Republic of Korea;* orcid.org/0009-0002-0235-6927

Kiman Park − *Department of Chemistry, University of Tennessee, Knoxville, Tennessee 37996, United States*

Emma Kirkman-Davis − *Carlson School of Chemistry and Biochemistry, Clark University, Worcester, Massachusetts 01610, United States*

Mark M. Turnbull − *Carlson School of Chemistry and Biochemistry, Clark University, Worcester, Massachusetts 01610, United States*

Minseong Lee − *National High Magnetic Field Laboratory, Los Alamos, New Mexico 87545, United States*

John Singleton − *National High Magnetic Field Laboratory, Los Alamos, New Mexico 87545, United States*

Stephen A. McGill − *National High Magnetic Field Laboratory, Tallahassee, Florida 32310, United States*

Heung-Sik Kim − *Department of Semiconductor Physics and Institute of Quantum Convergence Technology, Kangwon National University, Chuncheon 24341, Republic of Korea*

Complete contact information is available at: https://pubs.acs.org/10.1021/acs.inorgchem.5c00458

Author Contributions

◆A.L.B. and J.J. contributed equally to this work.

Notes

The authors declare no competing financial interest.

■ ACKNOWLEDGMENTS

Research at the University of Tennessee is supported by the National Science Foundation (CHM-2342425). Research at Clark University is funded by the National Science Foundation (IMR-0314773). E.K.-D. is grateful for support from the Frederick M. and Alice Murdock Summer Science Fellowship. J.H.L. and J.J. are supported by Midcareer Researcher (2020R1A2C2103126), Basic Research Laboratory (RS-2023-00218799), Nano and Material Technology Development Program (RS-2024-00404361), and RS-2023-00257666 through the National Research Foundation of Korea (NRF) funded by the Korea government (MSIT). This work was also supported by the Korea Institute for Advancement of Technology (KIAT) grant funded by the Korea Government (MOTIE) (P0023703, HRD Program for Industrial Innovation) and the National Supercomputing Center with supercomputing resources including technical support (KSC-2022-CRE-0075, KSC-2022-CRE-0454, KSC-2022-CRE-0456, KSC-2023-CRE-0547). H.-S.K. was supported by the Basic Science Research Program through the NRF funded by the Ministry of Science and ICT (MSIT) [Grant No. NRF-2020R1C1C1005900 and RS-2023-00220471]. The National High Magnetic Field Laboratory is supported by the National Science Foundation Cooperative Agreement DMR-2128556, the State of Florida, and the U.S. Department of Energy. We thank Ella Ye for photographing the crystals.

■ REFERENCES

(1) Liu, J.; Goddard, P. A.; Singleton, J.; Brambleby, J.; Foronda, F.; Möller, J. S.; Kohama, Y.; Ghannadzadeh, S.; Ardavan, A.; Blundell, S. J.; Lancaster, T.; Xiao, F.; Williams, R. C.; Pratt, F. L.; Baker, P. J.; Wierschem, K.; Lapidus, S. H.; Stone, K. H.; Stephens, P. W.; Bendix, J.; Woods, T. J.; Carreiro, K. E.; Tran, H. E.; Villa, C. J.; Manson, J. L. Antiferromagnetism in a family of S = 1 square lattice coordination polymers $NiX_2(pyz)_2$ (X = Cl, Br, I, NCS; pyz = Pyrazine). *Inorg. Chem.* **2016**, *55*, 3515−3529.

(2) Breunig, O.; Garst, M.; Klümper, A.; Rohrkamp, J.; Turnbull, M. M.; Lorenz, T. Quantum criticality in the spin-1/2 Heisenberg chain system copper pyrazine dinitrate. *Sci. Adv.* **2017**, *3*, No. eaao3773.

(3) Ghannadzadeh, S.; Möller, J. S.; Goddard, P. A.; Lancaster, T.; Xiao, F.; Blundell, S. J.; Maisuradze, A.; Khasanov, R.; Manson, J. L.; Tozer, S. W.; Graf, D.; Schlueter, J. A. Evolution of magnetic interactions in a pressure-induced Jahn-Teller driven magnetic dimensionality switch. *Phys. Rev. B* **2013**, *87*, No. 241102.

(4) Lancaster, T.; Goddard, P. A.; Blundell, S. J.; Foronda, F.; Ghannadzadeh, S.; Möller, J. S.; Baker, P. J.; Pratt, F. L.; Baines, C.; Huang, L.; Wosnitza, J.; McDonald, R. D.; Modic, K. A.; Singleton, J.; Topping, C. V.; Beale, T. A.; Xiao, F.; Schlueter, J. A.; Barton, A. M.; Cabrera, R. D.; Carreiro, K. E.; Tran, H. E.; Manson, J. L. Controlling

magnetic order and quantum disorder in molecule-based magnets. *Phys. Rev. Lett.* **2014**, *112*, No. 207201.
(5) Goddard, P. A.; Singleton, J.; Sengupta, P.; McDonald, R. D.; Lancaster, T.; Blundell, S. J.; Pratt, F. L.; Cox, S.; Harrison, N.; Manson, J. L.; Southerland, H. I.; Schlueter, J. A. Experimentally determining the exchange parameters of quasi-two-dimensional Heisenberg magnets. *New J. Phys.* **2008**, *10*, No. 083025.
(6) Wang, Z.-X.; Li, M.-X.; Shao, M.; Xiao, H.-P. A two-dimensional copper polymer constructed from rod-shaped ferromagnetic secondary building units. *Inorg. Chem. Commun.* **2009**, *12*, 201−203.
(7) Banks, M. G.; Kremer, R.; Hoch, C.; Simon, A.; Ouladdiaf, B.; Broto, J.-M.; Rakoto, H.; Lee, C.; Whangbo, M.-H. Magnetic ordering in the frustrated Heisenberg chain system cupric chloride $CuCl_2$. *Phys. Rev. B* **2009**, *80*, No. 024404.
(8) Brinzari, T. V.; Chen, P.; Sun, Q.-C.; Liu, J.; Tung, L.-C.; Wang, Y.; Schlueter, J.; Singleton, J.; Manson, J.; Whangbo, M.-H.; Litvinchuk, A. P.; Musfeldt, J. Quantum critical transition amplifies magnetoelastic coupling in $Mn[N(CN)_2]_2$. *Phys. Rev. Lett.* **2013**, *110*, No. 237202.
(9) Kono, Y.; Sakakibara, T.; Aoyama, C.; Hotta, C.; Turnbull, M.; Landee, C.; Takano, Y. Field-induced quantum criticality and universal temperature dependence of the magnetization of a spin-1/2 Heisenberg chain. *Phys. Rev. Lett.* **2015**, *114*, No. 037202.
(10) Vinslava, A.; Tasiopoulos, A. J.; Wernsdorfer, W.; Abboud, K. A.; Christou, G. Molecules at the quantum-classical nanoparticle interface: giant Mn_{70} single-molecule magnets of ∼ 4 nm diameter. *Inorg. Chem.* **2016**, *55*, 3419−3430.
(11) Sheu, Y.-M.; Chang, Y.; Chang, C.; Li, Y.; Babu, K.; Guo, G.; Kurumaji, T.; Tokura, Y. Picosecond creation of switchable optomagnets from a polar antiferromagnet with giant photoinduced Kerr rotations. *Phys. Rev. X* **2019**, *9*, No. 031038.
(12) Liu, J.; Kittaka, S.; Johnson, R.; Lancaster, T.; Singleton, J.; Sakakibara, T.; Kohama, Y.; Van Tol, J.; Ardavan, A.; Williams, B.; Blundell, S.; Manson, Z.; Manson, J.; Goddard, P. Unconventional field-induced spin gap in an S = 1/2 chiral staggered chain. *Phys. Rev. Lett.* **2019**, *122*, No. 057207.
(13) Narayan, A.; Cano, A.; Balatsky, A. V.; Spaldin, N. A. Multiferroic quantum criticality. *Nat. Mater.* **2019**, *18*, 223−228.
(14) Giamarchi, T. *Understanding Quantum Phase Transitions*; CRC Press: Taylor & Francis, 2010; p 291.
(15) Basov, D. N.; Averitt, R.; Hsieh, D. Towards properties on demand in quantum materials. *Nat. Mater.* **2017**, *16*, 1077−1088.
(16) Ghosh, S.; Datta, S.; Friend, L.; Cardona-Serra, S.; Gaita-Ariño, A.; Coronado, E.; Hill, S. Multi-frequency EPR studies of a mononuclear holmium single-molecule magnet based on the polyoxometalate $[Ho^{III}(W_5O_{18})_2]^{9-}$. *Dalton Trans.* **2012**, *41*, 13697−13704.
(17) Shiddiq, M.; Komijani, D.; Duan, Y.; Gaita-Ariño, A.; Coronado, E.; Hill, S. Enhancing coherence in molecular spin qubits via atomic clock transitions. *Nature* **2016**, *531*, 348−351.
(18) Zadrozny, J. M.; Gallagher, A. T.; Harris, T. D.; Freedman, D. E. A porous array of clock qubits. *J. Am. Chem. Soc.* **2017**, *139*, 7089−7094.
(19) Lancaster, T. Skyrmions in magnetic materials. *Contemp. Phys.* **2019**, *60*, 246−261.
(20) Yang, S.-H. Spintronics on chiral objects. *Appl. Phys. Lett.* **2020**, *116*, No. 120502.
(21) Bossini, D.; Pancaldi, M.; Soumah, L.; Basini, M.; Mertens, F.; Cinchetti, M.; Satoh, T.; Gomonay, O.; Bonetti, S. Ultrafast amplification and nonlinear magnetoelastic coupling of coherent magnon modes in an antiferromagnet. *Phys. Rev. Lett.* **2021**, *127*, No. 077202.
(22) Camsari, K. Y.; Sutton, B. M.; Datta, S. P-bits for probabilistic spin logic. *Appl. Phys. Rev.* **2019**, *6*, No. 011305.
(23) Bai, L.; Feng, W.; Liu, S.; Šmejkal, L.; Mokrousov, Y.; Yao, Y. Altermagnetism: Exploring new frontiers in magnetism and spintronics. *Adv. Funct. Mater.* **2024**, *34*, No. 2409327.
(24) Landee, C. P.; Turnbull, M. M. Recent developments in low-dimensional copper(II) molecular magnets. *Eur. J. Inorg. Chem.* **2013**, *2013*, 2266−2285.
(25) Hammar, P. R.; Stone, M.; Reich, D. H.; Broholm, C.; Gibson, P.; Turnbull, M.; Landee, C.; Oshikawa, M. Characterization of a quasi-one-dimensional spin-1/2 magnet which is gapless and paramagnetic for $g\mu_B H \lesssim J$ and $k_B T \ll J$. *Phys. Rev. B* **1999**, *59*, No. 1008.
(26) Lancaster, T.; Blundell, S.; Brooks, M.; Baker, P.; Pratt, F.; Manson, J. L.; Landee, C.; Baines, C. Magnetic order in the quasi-one-dimensional spin-1/2 molecular chain compound copper pyrazine dinitrate. *Phys. Rev. B* **2006**, *73*, No. 020410.
(27) Günaydın-Şen, Ö.; Lee, C.; Tung, L.; Chen, P.; Turnbull, M.; Landee, C.; Wang, Y.; Whangbo, M.-H.; Musfeldt, J. Spin-lattice interactions through the quantum critical transition in $Cu(pyz)(NO_3)_2$. *Phys. Rev. B* **2010**, *81*, No. 104307.
(28) Coldea, R.; Tennant, D.; Cowley, R.; McMorrow, D.; Dorner, B.; Tylczynski, Z. Quasi-1D S = 1/2 Antiferromagnet Cs_2CuCl_4 in a Magnetic Field. *Phys. Rev. Lett.* **1997**, *79*, No. 151.
(29) Starykh, O. A.; Katsura, H.; Balents, L. Extreme sensitivity of a frustrated quantum magnet: Cs_2CuCl_4. *Phys. Rev. B* **2010**, *82*, No. 014421.
(30) Roberts, S. A.; Bloomquist, D.; Willett, R.; Dodgen, H. Thermochromic phase transitions in copper (II) halide salts. 1. Crystal structure and magnetic resonance studies of isopropylammonium trichlorocuprate (II). *J. Am. Chem. Soc.* **1981**, *103*, 2603−2610.
(31) Blockmon, A. L.; Lee, M.; Zhang, S.; Manson, Z. E.; Manson, J. L.; Zapf, V. S.; Musfeldt, J. L. High field electrical polarization and magnetoelectric coupling in chiral magnet $[Cu(pym)(H_2O)_4]SiF_6 \cdot H_2O$. *Inorg. Chem.* **2024**, *63*, 11737−11744.
(32) Goddard, P. A.; Manson, J. L.; Singleton, J.; Franke, I.; Lancaster, T.; Steele, A. J.; Blundell, S. J.; Baines, C.; Pratt, F. L.; McDonald, R. D.; Ayala-Valenzuela, O. E.; Corbey, J. F.; Southerland, H. I.; Sengupta, P.; Schlueter, J. A. Dimensionality selection in a molecule-based magnet. *Phys. Rev. Lett.* **2012**, *108*, No. 077208.
(33) Kirkman-Davis, E.; Witkos, F. E.; Selmani, V.; Monroe, J. C.; Landee, C. P.; Turnbull, M. M.; Dawe, L. N.; Polson, M. I.; Wikaira, J. L.; Pyrazine-bridged, C. Pyrazine-bridged Cu(II) chains: diaquabis(*n*-methyl-2-pyridone)copper(II) perchlorate complexes. *Dalton Trans.* **2020**, *49*, 13693−13703.
(34) Kiria, P.; Hyett, G.; Binions, R. Solid state thermochromic materials. *Adv. Mater. Lett.* **2010**, *1*, 86−105.
(35) White, M. A.; LeBlanc, M. Thermochromism in commercial products. *J. Chem. Educ.* **1999**, *76*, No. 1201.
(36) Aburas, M.; Soebarto, V.; Williamson, T.; Liang, R.; Ebendorff-Heidepriem, H.; Wu, Y. Thermochromic smart window technologies for building application: A review. *Appl. Energy* **2019**, *255*, No. 113522.
(37) Hakami, A.; Srinivasan, S. S.; Biswas, P. K.; Krishnegowda, A.; Wallen, S. L.; Stefanakos, E. K. Review on thermochromic materials: development, characterization, and applications. *J. Coat. Technol. Res.* **2022**, *19*, 377−402.
(38) Berns, R. S. *Billmeyer and Saltzman's Principles of Color Technology*; John Wiley & Sons, 2019.
(39) Kongchoo, S.; Kantacha, A.; Saithong, S.; Wongnawa, S. Synthesis, crystal structure, and spectroscopic properties of Cu(II) complex with 14-membered hexaazamacrocyclic ligands. *J. Chem. Crystallogr.* **2016**, *46*, 222−229.
(40) Dobrowolska, M.; Tivakornsasithorn, K.; Liu, X.; Furdyna, J.; Berciu, M.; Yu, K.; Walukiewicz, W. Controlling the Curie temperature in (Ga, Mn)As through location of the Fermi level within the impurity band. *Nat. Mater.* **2012**, *11*, 444−449.
(41) Rice, W.; Ambwani, P.; Bombeck, M.; Thompson, J.; Haugstad, G.; Leighton, C.; Crooker, S. Persistent optically induced magnetism in oxygen-deficient strontium titanate. *Nat. Mater.* **2014**, *13*, 481−487.
(42) Holinsworth, B. S.; Sims, H.; Cherian, J.; Mazumdar, D.; Harms, N.; Chapman, B.; Gupta, A.; McGill, S.; Musfeldt, J. Magnetic

https://doi.org/10.1021/acs.inorgchem.5c00458
Inorg. Chem. 2025, 64, 12518−12526

field tunability of spin-polarized excitations in a high-temperature magnet. *Phys. Rev. B* **2017**, *96*, No. 094427.
(43) Fan, S.; Das, H.; Rébola, A.; Smith, K. A.; Mundy, J.; Brooks, C.; Holtz, M. E.; Muller, D. A.; Fennie, C. J.; Ramesh, R.; Schlom, D. G.; McGill, S.; Musfeldt, J. L. Site-specific spectroscopic measurement of spin and charge in $(LuFeO_3)_m/(LuFe_2O_4)_1$ multiferroic superlattices. *Nat. Commun.* **2020**, *11*, No. 5582.
(44) Lee, M.; Schönemann, R.; Zhang, H.; Dahlbom, D.; Jang, T.-H.; Do, S.-H.; Christianson, A. D.; Cheong, S.-W.; Park, J.-H.; Brosha, E.; Marcelo, J.; Barros, K.; Batista, C. D.; Zapf, V. S. Field-induced spin level crossings within a quasi-XY antiferromagnetic state in $Ba_2FeSi_2O_7$. *Phys. Rev. B* **2023**, *107*, No. 144427.
(45) Toth, J.; Bird, M. D.; Bole, S.; Gundlach, S.; O'Reilly, J. FEA-aided design of a powered scattering magnet at the NHMFL. *IEEE Trans. Appl. Supercond.* **2010**, *20*, 660−663.
(46) Kresse, G.; Joubert, D. From ultrasoft pseudopotentials to the projector augmented-wave method. *Phys. Rev. B* **1999**, *59*, No. 1758.
(47) Kresse, G.; Furthmüller, J. Efficiency of ab-initio total energy calculations for metals and semiconductors using a plane-wave basis set. *Comput. Mater. Sci.* **1996**, *6*, 15−50.
(48) Perdew, J. P.; Burke, K.; Ernzerhof, M. Generalized gradient approximation made simple. *Phys. Rev. Lett.* **1996**, *77*, No. 3865.
(49) Amft, M.; Burkert, T.; Sanyal, B.; Oppeneer, P. First-principles calculations of optical and magneto-optical properties of $Ga_{1-x}Mn_xAs$ and MnAs. *Phys. B* **2009**, *404*, 3782−3788.

https://doi.org/10.1021/acs.inorgchem.5c00458
Inorg. Chem. 2025, 64, 12518−12526